

The Synergistic Effects of Central Core Size and End Group Engineering on Performance of Narrow Bandgap Nonfullerene Acceptors

Xunfan Liao^{a,b}, Hongqiao Pei^a, Heng Zhao^c, Yongjie Cui^{a,b}, Lei Li^a, Xueliang Shi^b, Peipei Zhu^{*a},

Wei Ma^{*c}, Yiwang Chen^{*a} and Alex K.-Y. Jen^{*d}

^a Institute of Advanced Scientific Research (iASR) & Key Laboratory of Functional Small Molecules for Ministry of Education, Jiangxi Normal University, 99 Ziyang Avenue, Nanchang 330022, China

^b State Key Laboratory for Modification of Chemical Fibers and Polymer Materials, Donghua University, Shanghai 201620, China

^c State Key Laboratory for Mechanical Behavior of Materials, Xi'an Jiaotong University, Xi'an 710049, China

^d Department of Chemistry, City University of Hong Kong, Kowloon, Hong Kong

*Corresponding author.

E-mail address: ppzhu@jxnu.edu.cn (P. Zhu), msewma@xjtu.edu.cn (W. Ma), ywchen@ncu.edu.cn (Y. Chen), alexjen@cityu.edu.hk (A. Jen)

Keywords: ultra-narrow bandgap, nonfullerene acceptors, intramolecular charge transfer, core and end group, organic solar cells

Abstract:

Understanding the relationship between the molecular structure and photoelectric properties of fused-ring non-fullerene acceptors (NFAs) is of far-reaching significance to the development of

organic solar cells (OSCs). Herein, six NFAs based on multiple thiophenes (4T, 6T and 8T) are employed to systematically probe the synergistic effects of extending central core size and terminal fluorination. The absorption results manifest that the molecular absorption is comprehensively affected by molecular crystallinity, planarity, conjugation length and intramolecular electron push-pull effect, simultaneously. The intensity of electron push-pull effect is not only related to the electron-donating ability of central core and the electron-withdrawing ability of end group, but also may be related to the distance between the positive and negative centers. The extension of central core leads to the more planar backbone and stronger crystallinity of NFAs, and less energy loss (E_{loss}) in its based OSC. Compared with the extension of central core, terminal fluorination has a greater impact on molecular photoelectric properties. The terminal fluorination significantly enhances the push-pull effect, lowers the energy levels, and slightly increases the vibrational relaxation. As a result, the strongest crystallinity and coplanarity of 8TIC-4F lead to a low vibrational relaxation of 0.18 eV, which makes PTB7-Th:8TIC-4F device exhibit a small E_{loss} of 0.51 eV and a high efficiency of 10.4%. In addition, the fluorinated 6TIC-4F with suitable core size exhibits suitable energy level, absorption, crystallization, and phase separation morphology, making its as-cast device up to 11.61% efficiency. To the best of the authors' knowledge, the PCE of 11.61% for PTB7-Th:6TIC-4F based device without any treatment is one of the highest values reported for the NAFs with over 1000 nm absorption.

Keywords: nonfullerene acceptors, central core size, end group fluorination, push-pull effect, organic solar cells

1. Introduction:

As a promising alternative to conventional inorganic solar cells, such as silicon-based photovoltaic technology, organic solar cells (OSCs) show great potential for a cost-effective solar energy conversion platform with the advantages of low cost, solution processability, light weight and mechanical flexibility.¹⁻¹⁰ In particular, OSCs can be used for building integrated photovoltaics (BIPVs) and smart window technologies due to its semitransparent and are considered as one of the key business markets for future OSCs.¹¹⁻¹³ Developing narrow bandgap nonfullerene acceptors (NFAs) with strong absorption in the near-infrared (NIR) region and weak absorption in the visible range is an imperative avenue for achieving the efficient semitransparent OSCs. Thus, far, tremendous efforts have been involved in developing high-performance novel NIR NFAs and many have been reported due to the emergence of acceptor-donor-acceptor (A-D-A) type electron fused-ring acceptors (FREAs), such as Y6 series,¹⁴⁻¹⁹ IEICO-4F,²⁰ CO₈DFIC,²¹ F8IC and DTPC-4F,²²⁻²⁴ et al., which absorption even exceed 1000 nm and indicative of their great potential for organic photodetector applications.

The most straightforward ways to construct a redshifted NIR FREA is to reinforce intramolecular charge transfer (ICT) effect or increase intermolecular interactions. A stronger ICT effect can be induced by either or both enhancing the electron-donating ability of central core or enhancing the electron-withdrawing ability of end group to increase intramolecular electron push-pull effect.²⁵⁻³³ For example, compared to ITIC,³⁴ Hou and co-workers reported a more red-shifted acceptor IT-4F by introducing two halogen fluorine atoms onto the end group 1,1-dicyanomethylene-3-indanone (IC).³⁵ In general, terminal fluorination not only can enhance the ICT effect to broaden the absorption, but also can enhance the intra/intermolecular interaction due to the noncovalent

interactions of F...H, S...F, and so on, which improve the molecular crystallinity and facilitate charge transport.³⁶ Besides, fluorination simultaneously down-shifts the highest occupied molecular orbital (HOMO) and the lowest unoccupied molecular orbital (LUMO) levels, which affords increased energy offset for efficient exciton dissociation while the decreased LUMO energy is detrimental for open-circuit voltage (V_{OC}).³⁷⁻³⁹ On the other hand, Jen and co-workers have demonstrated a stronger central donor core of thiophene-thieno[3,2-b]thiophene-thiophene (4T) to replace the first generation core of indacenodithieno[3,2-b]thiophene (IDTT) and constructed a efficient NIR FREA 4ITC with absorption over 900 nm, which is significantly more redshifted than the IDTT core based star acceptor ITIC (800 nm).⁴⁰ In addition, the extension of the central core could also induce redshift of absorption, elevate both the HOMO and LUMO energy level, and enhance intermolecular π - π stacking. So far, although these two strategies have validity in constructing efficient NIR FREAs for OSCs and their respective effects on the photoelectric performance have also been preliminary studied, there are still many issues that need to be figured out. First, the law of the influence of central core length on absorption have not been systematically investigated and unclear to date, and whether the longer the central core, the more redshift of the absorption is still ambiguity. Besides, the relationship between energy loss ($E_{loss} = E_g - eV_{OC}$) and molecular structure is not yet clear and more systematic research is needed. Moreover, the influence of extending central core and modifying end groups on FREAs' performance have been studied individually, but systematically combined comparisons have rarely been explored. Under this situation, it is impossible to rationally compare these FREAs or properly understand how the chemical nature of the core size and end group would affect performance of the FREAs.

Taking aforementioned hurdles into consideration, in this work, we designed and synthesized a new fused core with eight thiophene rings (8T), which was end-capped with IC or fluorinated IC (DFIC) to afford two new FREAs, 8TIC and 8TIC-4F, respectively. These two new FREAs, together with our previously reported 4T and 6T based FREAs 4TIC,⁴⁰ 4TIC-4F,²³ 6TIC and 6TIC-4F to construct a library of structurally closely related FREAs (**Scheme 1a**).^{23, 41} With this small library, we are able to systematically investigate the effect of central core-extension, fluorination, and their combined effects on A-D-A type NIR NFAs, including their impact on photophysical and electronic properties, quantum chemistry calculation, film morphology, charge transport, E_{loss} and photovoltaic performance when paired with donor polymer PTB7-Th. We discover that the molecular absorption is comprehensively affected by molecular crystallinity, planarity, conjugation length and intramolecular electron push-pull effect, simultaneously, since that 4TIC, 4TIC-4F, 6TIC and 8TIC exhibit similar thin film absorption edges. Besides, either with the extension of central core or terminal fluorination, the degree of molecular absorption redshift in solution or film state gradually decreases. From the theoretical calculations and experimental results, we infer that the ICT effect is not only related to the amount of charge transfer, but also may be related to the distance between the positive and negative centers as well as molecular aggregation state. Moreover, compared with the extension of central core, terminal fluorination has a greater impact on molecular absorption, energy level, crystallization, film morphology and device E_{loss} . Terminal fluorination significantly increase the crystallinity of 6TIC-4F and 8TIC-4F, while 4TIC-4F shows the opposite result, its crystallinity becomes very poor and it is amorphous, which is rarely reported in fluorinated FREAs. As a result, the devices based on PTB7-Th:4TIC-4F exhibit a mediocre power conversion efficiency (PCE) of 7.25% with

a very low V_{OC} of 0.63 V due to its large device E_{loss} (0.76 eV). In comparison, the fluorinated 6TIC-4F with suitable core size exhibits suitable energy level, absorption, crystallization, and phase separation morphology, making its as-cast device up to 11.61% efficiency with a high J_{SC} of 24.4 mA/cm². When further extending the central core to eight thiophenes, the crystallinity and coplanarity of 8TIC-4F further increase, while the phase separation in blend film increases significantly along with decreased energy offset which is unbeneficial for exciton dissociation and charge transport, respectively, leading to a reduction of PCE (10.4%) of PTB7-Th:8TIC-4F device. It is worth mentioning that during our research, Zhan et al. also reported the same fluorinated 8T FREA (F10IC) as 8TIC-4F with an efficiency of 10.2%.²² Here, our study offers more understanding of relationship between molecular structure and performance by systematic deciphering the effects of extension of central core and end-group fluorination and provide guidelines for future high-performance FREAs design.

2. Results and Discussion

2.1. Synthesis and Characterization

The synthetic routes for 8TIC and 8TIC-4F are similar to those of our reported 4T and 6T based FREAs, as shown in **Scheme 1b**, and the synthesis details and characterization data are depicted in Supporting Information. The Stille coupling between diethyl 2,5-dichlorothieno[3,2-b]thiophene-3,6-dicarboxylate **1** and tributyl(dithieno[3,2-b:2',3'-d]thiophen-2-yl)stannane **2** gave compound **3** in over 85% yield. The double nucleophilic additions of (4-hexylphenyl)magnesium bromide Grignard reagent to compound **3** followed by amberlyst 15 induced Friedel–Crafts intramolecular cyclization afford

8T in 70% yield. The synthesis yield of 70% for 8T is much higher than that reported from Zhan's work (33%), who used the conditions of protic acid (acetic acid/H₂SO₄) catalyzed for Friedel-Crafts intramolecular cyclization.²³ 8T was then treated with Vilsmeier reagent to afford the 8T-CHO in 90% yield. Finally, 8TIC and 8TIC-4F were obtained as dark green solid in 85% and 82% yield, respectively, by Knoevenagel condensation reactions. The chemical structures of the intermediates and the target compounds were fully characterized by ¹H NMR, ¹³C NMR, and MALDITOF mass spectrometry (**Figure S1-S9** in the Supporting Information).

2.2. Electrochemical Properties

The HOMO and LUMO energy levels of the acceptors were measured by cyclic voltammetry (CV) measurements (**Figure S10**, Supporting Information). As shown in **Figure 1a** and **Table 1**, the HOMO and LUMO energy levels of 4TIC, 4TIC-4F, 6TIC, 6TIC-4F, 8TIC and 8TIC-4F were calculated to be -5.56/-4.03, -5.60/-4.21, -5.42/-3.91, -5.45/-4.14, -5.30/-3.72, and -5.36/-3.88 eV, respectively, indicating that extending the central core could upshift both HOMO and LUMO energy levels while terminal fluorination could downshift both HOMO and LUMO energy levels. Although previous works have demonstrated that small HOMO offsets are sufficient for hole transfer from A to D, the HOMO offset of PTB7-Th and 8TIC was too small (0.1 eV) to offer enough driving force for charge dissociation in PTB7-Th:8TIC based device, which was detrimental to *J*_{SC} and PCE.

2.3. Optical Properties

The optical absorption of the six acceptors was investigated with UV-vis-NIR spectroscopy. As we

know that the main factors affecting molecular absorption are the ICT effect and intermolecular interactions. So, the terminal fluorination and extension of central core could change the absorption and the magnitude of their respective contributions is worth investigating. In dichloromethane (DCM) solution state, as shown in **Figure 1b**, all six acceptors exhibit strong and wide absorption in the range of 550–800 nm. With the extension of central core or terminal fluorination, the absorption of the acceptors gradually red-shifted, and the degree of molecular absorption redshift gradually decreases. Besides, compared to the extension of central core, terminal fluorination leads to more absorption redshift both in solution and film state, implying terminal fluorination could induce stronger ICT effect or intermolecular interactions, which will be discussed in the part of theoretical calculations. The similar change trend also appears in the film absorption. As shown in **Figure 1c**, the thin films of all six acceptors show red-shifted and broadened absorption spectra with onset at 886–984 nm relative to their solutions, which indicative of stronger molecular packing in each film state. Besides, in solution state, 4TIC-4F is significantly red-shifted relative to 4TIC, while its absorption is almost unchanged in film state. This may be related to the poor crystallinity of 4TIC-4F, and it proves that the molecular packing has a very significant influence on the absorption (*vide infra*). Interestingly, 4TIC, 6TIC with 8TIC, and 6TIC-4F with 8TIC-4F exhibit similar thin film absorption edges, respectively, indicating little difference in corresponding ICT effects. The result manifests that the intensity of ICT effect is not only related to the electron-donating ability of central core and the electron-withdrawing ability of end group, but also may be related to the distance between the positive and negative centers. Moreover, in comparison to 6TIC and 8TIC, 6TIC-4F and 8TIC-4F exhibit obvious absorption redshift, respectively, which result from their improved molecular

crystallinity and enhanced ICT effects. The optical bandgaps (E_g^{opt}) were determined to be 1.40, 1.39, 1.38, 1.27, 1.37, and 1.26 eV for 4TIC, 4TIC-4F, 6TIC, 6TIC-4F, 8TIC and 8TIC-4F from the absorption onsets in films, respectively. The absorption properties are summarized in **Table 1**.

2.4. Theoretical Calculations

To study the ICT effect in FREAs and explain the changes in the absorption of the six acceptors, the absorption spectra in chloroform solution and light excited inter-fragment (D→A) charge transfer (IFCT) characteristics were calculated at PBE0/def2tzvp time-dependent DFT (TD-DFT) (nstates = 50) IOp(9/40 = 4) based on the optimized geometries and the wave functions were then analyzed by Multiwfn 3.7(dev) program,⁴² as shown in **Figure S11**, **S12**, and **Figure 2a-b**. In addition, electrostatic potential (ESP) and molecular polarization index (MPI) calculation were used to further analyze the difference in ICT and self-assembly behavior of FREAs,⁴³ as shown in **Figure 2c-g** and **Table S1**. The hexyl groups of the six acceptors were replaced by methyl to simplify the calculations. The calculation results show that the net charge transfer amount increases with the extension of donor cores, and is significantly stronger than the effect of fluorination. It is worth noting that although molecular IFCT is enhanced, the increase is gradually reduced, indicating that further extending the conjugate length will not lead to significant red-shift, which is consistent with the measured absorption changes in the solution and film state. Furthermore, the increase of charge transfer caused by fluorination is small, but the actual absorption is significantly red-shifted. There may be two reasons. First, fluorination causes the increase of MPI, resulting in the enhancement of molecular polarity and uneven charge distribution in molecules, which can be verified from the distribution of ESP value. Moreover, the introduction of fluorine atom induces charge transfer to the terminals and promotes the charge

transfer between the terminal of molecules. The second is that there are some molecular aggregation and orderly accumulation in the solution state, and the intermolecular accumulation is improved after the introduction of fluorine atom. The ICT effect may be enhanced due to the more ordered molecular accumulation in the film state, and its change law could be similar to that in the solution state. However, more systematic studies are needed in the future to quantify the affecting factors (e.g., distance between positive and negative charge center, and charge transfer amount, etc.) on the ICT effect and thus outside the focus of the current study.

2.5. Molecular Packing and Crystalline Properties

As mentioned above, the absorption of the acceptor film is not only related to the effect of ICT, but also closely related to its film crystallinity and molecular packing. Here, in order to verify whether the almost unchanged absorption of 4TIC-4F compared to 4TIC is due to the poor crystallinity of 4TIC-4F, and to study the influence of terminal fluorination and extension of central core on the molecular crystallinity, we performed the grazing incidence wide-angle X-ray scattering (GIWAXS) measurements of neat films. The 2D GIWAXS patterns and cut-line profiles of NFAs neat film in in-plane and out-plane direction are shown in **Figure 3** and corresponding parameters are summarized in **Table S2**. As we speculated, the neat 4TIC-4F film shows very weak (010) diffuse rings, indicative of isotropic and disordered packing, which is rarely reported in fluorinated FREAs. We have tried to explain this special change by culturing 4TIC-4F single crystals, but failed. We found that 4TIC-4F could not form crystals, but formed a kind of floccule. The poor crystallinity and disordered packing of 4TIC-4F prove that the molecular packing has a very significant influence on the absorption and the amorphous nature of 4TIC-4F also could lead

to low charge mobility and high E_{loss} (vide infra). In contrast, the textures of the other five acceptors are remarkably different from that of 4TIC-4F. Specifically, a well-defined (010) reflection peak at $q \approx 1.77 \text{ \AA}^{-1}$ only appears in the out-of-plane (OOP) direction, indicating the preferential face-on ordering of the five acceptors. In addition, with the extension of central core, the d-spacing calculated from (010) OOP peaks of 4TIC ($d = 4.42 \text{ \AA}$), 6TIC ($d = 3.63 \text{ \AA}$) to 8TIC ($d = 3.56 \text{ \AA}$) neat film is reduced gradually, suggesting the tighter π - π stacking from 4TIC, 6TIC to 8TIC. Terminal fluorination will further reduce the d-spacing and increase the coherence length (CL), indicating the tighter and stronger π - π stacking in 6TIC-4F ($d = 3.54 \text{ \AA}$, $\text{CL} = 29.0 \text{ \AA}$) and 8TIC-4F ($d = 3.53 \text{ \AA}$, $\text{CL} = 30.7 \text{ \AA}$). In particular, 8TIC-4F exhibits the best ordered due to the most pronounced OOP (010) π - π stacking and the strongest scattering intensities peak along with disappeared OOP (100) peak, suggesting a highly face-on crystal orientation with respect to the substrate and the best planarity, which is agree well with the DFT calculation results (**Figure S13** in supporting information). The highly face-on crystal orientation also was found in 8TIC since its OOP (100) peak also disappeared. These results elucidate that the extension of central core not only can increase the molecular crystallinity and reduce π - π stacking distance, but also can increase the face-on crystal orientation. In addition, compared with the extension of central core, terminal fluorination has a greater impact on the molecular crystallinity. Moreover, with the extension of central core, the change of molecular crystallinity is gradually reduced. The crystallinity of 8T and 6T acceptors has little change, while the crystallinity of 6T acceptors is significantly higher than that of 4T acceptors. Thus, further extending the central core (more than 8T) will result in few changes on molecular crystallinity and packing. The above results also explain why the absorption edges of 6T and 8T acceptors are similar.

2.6. Photovoltaic Performance

To investigate the photovoltaic performance of the FREAs derived solar cells, bulk-heterojunction (BHJ) devices were fabricated with a conventional structure of ITO/PEDOT:PSS/PTB7-Th:acceptor/C₆₀-bis/Ag, where C₆₀-bis is the bis-fulleropyrrolidinium iodide salt.⁴⁴ The molecular structure of C₆₀-bis and the device structure are presented in **Figure 4a** and **b**, respectively. In order to inhibit excessive molecular aggregation in active layer due to too strong crystallinity of the 6T and 8T acceptors, we selected chloroform as solvent and used dynamic drop-casting to form the blend film (**Figure 4c**). This film forming strategy which has been widely employed in Y6 and its derivatives system can reduce the crystallization time of the active layer, so that it can crystallize quickly and reach a thermodynamic equilibrium state. All the devices were fabricated with the same conditions, which the D:A ratio is 1:1.7 and the blend film were processed without any optimization treatment. The current density–voltage (J – V) curves of the six FREAs based OSCs are shown in **Figure 4d**, and the detailed parameters with the best photovoltaic performance are presented in **Table 2**. From 4TIC to 6TIC and 8TIC based devices, the values of V_{OC} are increased from 0.78 to 0.81 and 0.86 V, the enhanced V_{OC} is attributed to the upshifted LUMO energy level. This trend of change also occurs in 4TIC-4F (0.63 V), 6TIC-4F (0.67 V) and 8TIC-4F (0.75 V) based devices, Notably, the V_{OC} of 0.75 V for 8TIC-4F is the highest value for the binary OSCs with the absorption onset close to 1000 nm. The 4TIC based device exhibits a moderate PCE of 8.91%, with a J_{SC} of 17.3 mA cm⁻² and an FF of 0.66. The PCE of 4TIC-4F device is significantly inferior to the 4TIC counterpart due to the obviously reduced V_{oc} . When extend the central core (from 4T to 6T) and simultaneously fluorinate

terminals, the resulting 6TIC-4F molecular device delivers an optimal PCE of 11.61%, with a high J_{SC} of 24.4 mA cm⁻² and a high FF of 0.71. It should be noted that the PCE of 11.61% for PTB7-Th:6TIC-4F based device without any treatment is one of the highest values reported for the NAFs with over 1000 nm absorption. When further extending the central core to 8T, the 8TIC and 8TIC-4F devices exhibit a decreased PCE of 6.2% and 10.4%, respectively. The significant reduced PCE and J_{SC} (13.1 mA cm⁻²) of 8TIC device may due to the small energy offset of donor and acceptor, which is unbeneficial for exciton dissociation and charge transport. The varied J_{SC} values were also confirmed by measuring their external quantum efficiencies (EQEs) (**Figure 4e**). The J_{SC} values calculated from the EQE curves are 16.7, 17.2, 18.8, 23.4, 12.8 and 20.2 mA cm⁻² for 4TIC, 4TIC-4F, 6TIC, 6TIC-4F, 8TIC and 8TIC-4F based devices, respectively, which are within reasonable difference to the J_{SC} values obtained from the corresponding $J-V$ curves. The highest J_{SC} of 6TIC-4F based device is owing to its strong and extended photoelectron response from 350 to 1000 nm. The E_{loss} of the 4TIC, 4TIC-4F, 6TIC, 6TIC-4F, 8TIC, and 8TIC-4F based devices is 0.62, 0.76, 0.57, 0.60, 0.51 and 0.51 eV, respectively. We can see that the E_{loss} decreases as the central core size of the acceptor increases. Meanwhile, we confirm that the crystallinity is closely related to E_{loss} . As the crystallinity increases, the E_{loss} of 8TIC-4F is as small as 8TIC, while the E_{loss} of 4TIC-4F is the largest due to its amorphous nature, so its V_{OC} drops significantly. More details and the investigation of E_{loss} will be discussed later.

2.7. Recombination Dynamics

To study the charge recombination behaviors of the six FREAs-based devices, the light intensity dependent J_{SC} and V_{OC} were investigated (**Figure 4f and g**). In general, the relationship between

J_{SC} and light intensity (P) can be described as an equation of $J_{SC} \propto P_{light}^\alpha$. The slope of the curve (α) should be equal to 1 if all dissociated free carriers are collected at the corresponding electrodes without charge recombination, while $\alpha < 1$ indicates the presence of some extent of bimolecular recombination.^{45, 46} As shown in **Figure 4f**, The α values of 4TIC, 4TIC-4F, 6TIC, 6TIC-4F, 8TIC and 8TIC-4F based devices are 0.952, 0.942, 0.958, 0.982, 0.904, and 0.963, respectively. It indicates that the 6TIC-4F based device can sweep out charge carriers most efficiently with negligible bimolecular recombination compared to that of other five devices, which supports the highest J_{SC} and FF obtained in its based device. In addition, as showed in **Figure 4g**, the slope of the dependence of V_{OC} on the light intensity were determined to be 1.32, 1.37, 1.34, 1.25, 1.44 and 1.31 kT/q for 4TIC, 4TIC-4F, 6TIC, 6TIC-4F, 8TIC and 8TIC-4F based devices, respectively, also indicating less trap-assisted recombination having occurred in the 6TIC-4F based device.

2.8. Charge Mobility

Space charge limited current (SCLC) method was conducted to investigate charge transport properties.⁴⁷ The charge carriers mobility of PTB7-Th:4TIC, PTB7-Th:4TIC-4F, PTB7-Th:6TIC, PTB7-Th:6TIC-4F, PTB7-Th:8TIC and PTB7-Th:8TIC-4F blend films were studied by constructing electron-only devices (ITO/ZnO/PTB7-Th:acceptor/C₆₀-bis/Ag) and hole-only devices (ITO/PEDOT:PSS/PTB7-Th:acceptor/MoO₃/Ag) (**Figure 5a** and **b**, and **Table 2**). The hole (μ_h) and electron (μ_e) mobilities for PTB7-Th:4TIC, PTB7-Th:4TIC-4F, PTB7-Th:6TIC, PTB7-Th:6TIC-4F, PTB7-Th:8TIC and PTB7-Th:8TIC-4F blend films were calculated to be $2.46 \times 10^{-4}/1.62 \times 10^{-4}$, $1.8 \times 10^{-4}/3.17 \times 10^{-5}$, $2.81 \times 10^{-4}/1.91 \times 10^{-4}$, $3.15 \times 10^{-4}/2.42 \times 10^{-4}$, $1.23 \times 10^{-4}/1.05 \times 10^{-5}$ and $2.21 \times 10^{-4}/1.26 \times 10^{-4} \text{ cm}^2 \text{ V}^{-1} \text{ s}^{-1}$, with μ_h/μ_e of 1.52, 5.68, 1.47, 1.3, 11.71

and 1.75, respectively. PTB7-Th:4TIC-4F blend film displays very low electron mobility, most likely ascribes to the weak intermolecular interaction, in accord with the amorphous nature of 4TIC-4F. Besides, PTB7-Th:8TIC blend film exhibits the lowest hole and electron mobility due to the small energy offset of donor and acceptor, which leads to the smallest J_{SC} and FF. Compared with the other five devices, the higher and more balanced charge mobilities of the PTB7-Th:6TIC-4F device favored exciton dissociation and charge transport, leading to the significantly enhanced J_{SC} and FF.

2.9. Photoluminescence Quenching Effect

The photoluminescence (PL) quenching effect ($\Delta PL = \frac{PL_{neat} - PL_{blend}}{PL_{neat}}$) were measured to elucidate the exciton dissociation and charge transfer behavior in PTB7-Th:4TIC, PTB7-Th:4TIC-4F, PTB7-Th:6TIC, PTB7-Th:6TIC-4F, PTB7-Th:8TIC and PTB7-Th:8TIC-4F based blends, where excitation wavelengths are 600 nm for PBT7-Th and 760 nm for 4TIC, 4TIC-4F, 6TIC, 6TIC-4F, 8TIC and 8TIC-4F. As shown in **Figure 5c**, when excited at 600 nm, the PL spectra were highly quenched for PTB7-Th:4TIC ($\Delta PL_{max} = 90.1\%$), PTB7-Th:4TIC-4F ($\Delta PL_{max} = 90.3\%$), PTB7-Th:6TIC ($\Delta PL_{max} = 94.4\%$) and PTB7-Th:6TIC-4F ($\Delta PL_{max} = 95.2\%$) based acceptors, indicating that the electron could effectively transfer from polymer donor PTB7-Th to these acceptors. The ΔPL_{max} value of the PTB7-Th:8TIC film was much smaller ($\Delta PL_{max} = 73.6\%$) than others due to its small driving force (0.13 eV) for electron dissociation. For the acceptor neat films, the broad emission peaks were observed in the range of 800-1200 nm when excited at 760 nm. Obviously, the PL emissions of the 4T and 6T based acceptors were effectively quenched, indicative of effective hole transfer from the acceptors to polymer donor PTB7-Th. With the

extension of central core, the PL quenching efficiency gradually decreased and the ΔPL_{\max} of 8TIC and 8TIC-4F significantly attenuated to 49.5% and 66.3%, respectively. This is because the driving force (0.1 eV for 8TIC and 0.16 eV for 8TIC-4F) is much less than the empirical low threshold of 0.3 eV between the HOMO levels of PTB7-Th and the acceptor, and is insufficient for hole transfer, subsequently leading to decreased J_{SC} and PCE.

2.10. Morphology Studies

The morphology of a blend film plays a vital role in determining its OSC performance. Thus, a systematic morphological study including of structural order and phase separation was performed by atomic force microscopy (AFM), transmission electron microscopy (TEM), GIWAXS and resonant soft X-ray scattering (RSoXS) measurements. As shown in **Figure 6a**, the root-mean-square (RMS) roughness for PTB7-Th:4TIC, PTB7-Th:4TIC-4F, PTB7-Th:6TIC, PTB7-Th:6TIC-4F, PTB7-Th:8TIC and PTB7-Th:8TIC-4F blend films are 0.82, 1.25, 1.02, 1.29, 1.16 and 1.44 nm, respectively, suggesting all the blend films displays smooth and uniform surface. The smooth and uniform surface also indicates good miscibility between the donor and acceptors, which is beneficial for contact between active layer and top electrode. Besides, we can see that the extension of central core and terminal fluorination both can increase the RMS roughness. In TEM images as shown in **Figure 6b**, PTB7-Th:6TIC-4F and PTB7-Th:8TIC-4F blend films exhibits clearer fibrous features and interpenetrating network framework than other blend films. The better morphology features of 6TIC-4F based blend film is beneficial for effective exciton dissociation and charge transport. However, the phase separation in 8TIC-4F blend film increases significantly, which is detrimental for exciton dissociation and charge transport, leading to a lower PCE in contrast to 6TIC-4F counterpart devices.

The difference in surface roughness and phase separation of the active layer should be closely related to the molecular crystallinity and molecular packing. Thus, grazing incidence wide-angle X-ray scattering (GIWAXS) measurement was employed to investigate the blend film crystallinity and molecular packing information. The 2D GIWAXS patterns and cut-line profiles in in-plane and out-plane direction were shown in **Figure 7** and corresponding parameters were summarized in **Table 3**. The (010) out-of-plane d-spacing and coherence length (CL) of PTB7-Th:4TIC, PTB7-Th:4TIC-4F, PTB7-Th:6TIC, PTB7-Th:6TIC-4F, PTB7-Th:8TIC and PTB7-Th:8TIC-4F blend films were calculated to be 4.59/11.4, 4.41/22.0, 4.47/9.8, 3.97/15.1, 4.54/10.1 and 4.02/18.2 Å, respectively. Similarly to the results of the crystallinity analysis of the FREAs' neat film (**Figure 3**), terminal fluorination also strengthened intermolecular interaction, reduced the π - π stacking distance and increased the CL in blend films, which is crucial for high charge mobility and FF. In comparison to 4T based blends, the π -extended and fluorinated acceptors (6TIC-4F and 8TIC-4F) have smaller π - π stacking distances, with stronger π - π stacking (010) peaks at 1.582 and 1.562 Å⁻¹, respectively, which is conducive to charge transport. However, with the extension of central core and terminal fluorination, the lamellar d-spacing and CL of blend films calculated from (100) in-plane peaks significantly increased, especially for PTB7-Th:8TIC-4F blend (d = 22.51 Å, CL = 88.6 Å). The much larger lamellar d-spacing and CL of PTB7-Th:8TIC-4F could induce severely phase separation, which also might explain the lower carrier mobility of PTB7-Th:8TIC-4F than PTB7-Th:6TIC-4F.

The spatial dimensions of the phase-separated domains were further investigated by resonant soft

X-ray scattering (R-SoXS) analysis.^{48, 49} We have employed the R-SoXS measurements at different energy (270, 282, 283, 284.2, 284.8, 285.2, 285.8, 286.8 eV) near the carbon absorption edge to get the high contrast. Finally, we found the scattering at 284.8 eV get the highest contrast. The R-SoXS profiles at 270 eV was also presented in Supporting Information (**Figure S14**). **Figure 8** presents the R-SoXS profiles of the six blend films. The mode of the distribution S_{mode} of the scattering corresponds to the characteristic mode length scale, ξ of the corresponding log-normal distribution in real space with $\xi = 1/S_{\text{mode}}$. The characteristic mode length scale ξ (the distance between two donor domains or two acceptor domains) is estimated by the equation of $\xi = 2\pi/q_{\text{mode}}$, and the mode domain size is the half of ξ . The length scale of 22.67, 35.28 and 26.6 nm domain spacing are observed for PTB7-Th:4TIC ($q = 0.277 \text{ nm}^{-1}$), PTB7-Th:6TIC ($q = 0.178 \text{ nm}^{-1}$) and PTB7-Th:8TIC ($q = 0.236 \text{ nm}^{-1}$) blend films. Generally, introducing fluorine atoms in molecules can enhance intermolecular interactions, increase molecular aggregation, and thus increases phase separation of blend film. Nevertheless, compared to 4TIC blend, the fluorinated 4TIC-4F blend exhibits smaller domain spacing (16.10 nm), which is ascribe to its weak crystallinity. With the extension of central and terminal fluorination, the domain spacing of 6TIC-4F and 8TIC-4F are significantly increased to 50.65 and 93.73 nm, corresponding to domain size of 25.33 and 46.87 nm, respectively. It should be noted that the ideal domain size of active layer for efficient exciton diffusion and dissociation is around 20 nm, thus the severely phase separation was confirmed in PTB7-Th:8TIC-4F blend could subsequently induce ineffective charge transfer and comparatively higher bimolecular recombination, which is agreement with the results of TEM and GIWAXS. On the contrary, the PTB7-Th:6TIC-4F blend featuring strong crystallinity associating with broad spectral response, suitable energy level and ideal phase

separation morphology, ultimately contributing to the best PCE, J_{SC} and FF in its based OSCs.

2.11. Energy Loss

At last, we studied the relationship between molecular structure and energy loss. As we know, as a part of energy loss, the energetic loss caused by vibrational relaxation is inevitable and it can be figured out by calculating molecular Stokes shifts.⁵⁰ As shown in **Figure 9**, taking the absorption and PL edges in long wavelength region into consideration, the energetic loss caused by vibrational relaxation is 0.12, 0.25, 0.20, 0.22, 0.18 and 0.18 eV for 4TIC, 4TIC-4F, 6TIC, 6TIC-4F, 8TIC and 8TIC-4F, respectively. It can be seen from the above results that fluorination will increase the energetic loss caused by vibration relaxation, and 4TIC-4F exhibits the largest value of 0.25 eV, which is caused by its poor molecular crystallinity. When extending the conjugated central core, the coplanarity of the molecule increases and the energetic loss caused by fluorination is gradually reduced, and when the central core extends to 8T, the energetic loss of 8TIC is the same as that of 8TIC-4F. The insets in **Figure 9** are the energy levels diagram of ground states and excitation states for the six systems devices. The free charges are generated through a thermodynamical driven process from an excitation state to charge separation state and then get output voltage. In this process, another part of energy loss will occur. This part of energy loss is the energetic offsets between their excitation state and eV_{OC} .⁵¹ The magnitude of the energetic offsets plays a vital role in the charge separation efficiency. In the study of photovoltaic performance part, the total E_{loss} of the 4TIC, 4TIC-4F, 6TIC, 6TIC-4F, 8TIC, and 8TIC-4F based devices has been calculated to be 0.62, 0.76, 0.57, 0.60, 0.51 and 0.51 eV, respectively. Thus, the calculated energetic offsets for the 4TIC, 4TIC-4F, 6TIC, 6TIC-4F, 8TIC, and 8TIC-4F based

devices are 0.50, 0.51, 0.37, 0.38, 0.33 and 0.33 eV, respectively. Clearly, after the vibrational relaxation, the PTB7-Th:8TIC and PTB7-Th:8TIC-4F blends reserve less energy for charge separation, that explains why the charge separation efficiency of the two blends is relative lower than other blends, agreeing well with the PL results. The above results also explain why 8T acceptors exhibit lower device performance than the 6T acceptors. Additionally, the extension of the central core and the improvement of molecular order are conducive to reducing energy loss.

3. Conclusion

In summary, the synergistic effects of central core size and terminal fluorination on the performance of a series of multiple thiophene (4T, 6T and 8T) based nonfullerene acceptors have been systematically investigated. 4TIC, 4TIC-4F, 6TIC and 8TIC exhibit similar thin film absorption edges of ~890 nm. From the theoretical analysis and the result of molecular absorption, we infer that the ICT effect is not only related to the amount of charge transfer, but also may be related to the distance between the positive and negative centers. Extending the central core is effective in improving molecular coplanarity and reducing E_{loss} in its based OSCs. Besides, the extension of central core not only can increase the molecular crystallinity and reduce π - π stacking distance, but also can increase the face-on crystal orientation, which is conducive to charge transport. Compared with the extension of central core, terminal fluorination has a greater impact on molecular absorption, energy level, crystallinity, film morphology and vibrational relaxation. The change degree of molecular absorption, crystallinity and vibrational relaxation gradually decreases with the further extension of the conjugated length, and when a certain length is reached, the change will reach saturation. Therefore, 6TIC-4F and 8TIC-4F display very strong crystallinity

and similar absorption, and PTB7-Th:8TIC-4F device exhibit the smallest E_{loss} of 0.51 eV, a high efficiency of 10.4% and a high V_{OC} of 0.75 eV, which are better than that of the most ultra-narrow bandgap acceptors (absorption over 1000 nm). However, the small driving force for charge separation and relatively large phase separation of blend film limit the further improvement of its performance. In comparison, 6TIC-4F with suitable energy level, absorption, crystallinity, and phase separation morphology, making its as-cast device up to 11.61% efficiency, which is one of the highest values reported for the as-cast device based on the NAFs with over 1000 nm absorption. Taken all together, our study offers more understanding of relationship between molecular structure and performance by systematic deciphering the effects of extension of central core and end-group fluorination and provide guidelines for future high-performance FREAs design.

Declaration of Competing Interest

The authors declare no conflict of interest.

Acknowledgements

This work was financially supported by the National Natural Science Foundation of China (NSFC) (51973032, 21905043, 51833004 and 21875182), the “Chenguang Program” supported by Shanghai Education Development Foundation and Shanghai Municipal Education Commission (19CG36), Shanghai Sailing Program (19YF1401000), the Jiangxi Provincial Natural Science Foundation (20212ACB203005 and 20212BAB213018), the Thousand Talents Plan of Jiangxi Province (jxsq2019101051), the State Key Laboratory for Modification of Chemical Fibers and

Polymer Materials, Donghua University (KF2007), and 111 project 2.0 (BP2018008). X-ray data was acquired at beamlines 7.3.3 and 11.0.1.2 at the Advanced Light Source, which is supported by the Director, Office of Science, Office of Basic Energy Sciences, of the U.S. Department of Energy under Contract No. DE-AC02-05CH11231. The authors thank Chenhui Zhu at beamline 7.3.3, and Cheng Wang at beamline 11.0.1.2 for assistance with data acquisition.

References

- [1] L. Meng, Y. Zhang, X. Wan, C. Li, X. Zhang, Y. Wang, X. Ke, Z. Xiao, L. Ding, R. Xia, H. Yip, Y. Cao, Y. Chen, *Science* 361 (2018) 1094-1098.
- [2] W. Huang, P. Cheng, Y. M. Yang, G. Li, Y. Yang, *Adv. Mater.* 30 (2018) 1705706.
- [3] Y. Huang, E. J. Kramer, A. J. Heeger, G. C. Bazan, *Chem. Rev.* 114 (2014) 7006-7043.
- [4] N. Gasparini, A. Wadsworth, M. Moser, D. Baran, I. McCulloch, C. J. Brabec, *Adv. Energy Mater.* 8 (2018) 1703298.
- [5] G. Xu, X. Hu, X. Liao, Y. Chen, *Chin. J. Polym. Sci.* 39 (2021) 1441-1447.
- [6] X. Liao, F. Wu, Y. An, Q. Xie, L. Chen, Y. Chen, *Macromol. Rapid Commun.* 38 (2017) 1600556.
- [7] H. Sun, B. Liu, Y. Ma, J. Lee, J. Yang, J. Wang, Y. Li, B. Li, K. Feng, Y. Shi, B. Zhang, D. Han, H. Meng, L. Niu, B. Kim, Q. Zheng, X. Guo, *Adv. Mater.* 33 (2021) 2102635.
- [8] R. Ma, Y. Tao, Y. Chen, T. Liu, Z. Luo, Y. Guo, Y. Xiao, J. Fang, G. Zhang, X. Li, X. Guo, Y. Yi, M. Zhang, X. Lu, Y. Li, H. Yan, *Sci China Chem.* 64 (2021) 581-589.
- [9] H. Wang, Z. Zhang, J. Yu, X. Liu, W. Tang, *Chem. Eng. J.* 418 (2021) 129539.
- [10] Q. Liu, Y. Jiang, K. Jin, J. Qin, J. Xu, W. Li, J. Xiong, J. Liu, Z. Xiao, K. Sun, S. Yang, X.

- Zhang, L. Ding, *Sci. Bull.* 65 (2020) 272-275.
- [11] M. Batmunkh, Y. L. Zhong, H. Zhao, *Adv. Mater.* 32 (2020) 2000631.
- [12] C. J. M. Emmott, J. A. Röhr, M. Campoy-Quiles, T. Kirchartz, A. Urbina, N. J. Ekins-Daukes, J. Nelson, *Energy Environ. Sci.* 8 (2015) 1317-1328.
- [13] E. Ravishankar, R. E. Booth, C. Saravitz, H. Sederoff, H. W. Ade, B. T. O'Connor, *Joule* 4 (2020) 490-506.
- [14] J. Yuan, Y. Zhang, L. Zhou, G. Zhang, H.-L. Yip, T.-K. Lau, X. Lu, C. Zhu, H. Peng, P. A. Johnson, M. Leclerc, Y. Cao, J. Ulanski, Y. Li, Y. Zou, *Joule* 3 (2019) 1140-1151.
- [15] Z. Zhou, W. Liu, G. Zhou, M. Zhang, D. Qian, J. Zhang, S. Chen, S. Xu, C. Yang, F. Gao, H. Zhu, F. Liu, X. Zhu, *Adv. Mater.* 32 (2019) 1906324.
- [16] F. Qi, K. Jiang, F. Lin, Z. Wu, H. Zhang, W. Gao, Y. Li, Z. Cai, H. Woo, Z. Zhu, A. K.-Y. Jen, *ACS Energy Lett.* 6 (2021) 9-15.
- [17] Y. Cui, H. Yao, J. Zhang, K. Xian, T. Zhang, L. Hong, Y. Wang, Y. Xu, K. Ma, C. An, C. He, Z. Wei, F. Gao, J. Hou, *Adv. Mater.* 32 (2020) 1908205.
- [18] H. Chen, H. Lai, Z. Chen, Y. Zhu, H. Wang, L. Han, Y. Zhang, F. He, *Angew. Chem. Int. Ed.* 60 (2021) 3238-3246.
- [19] G. Li, X. Zhang, L. O. Jones, J. M. Alzola, S. Mukherjee, L. Feng, W. Zhu, C. L. Stern, W. Huang, J. Yu, V. K. Sangwan, D. M. DeLongchamp, K. L. Kohlstedt, M. R. Wasielewski, M. C. Hersam, G. C. Schatz, A. Facchetti, T. J. Marks, *J. Am. Chem. Soc.* 143 (2021) 6123-6139.
- [20] H. Yao, Y. Cui, R. Yu, B. Gao, H. Zhang, J. Hou, *Angew. Chem. Int. Ed.* 56 (2017) 3045-3049.
- [21] Z. Xiao, X. Jia, D. Li, S. Wang, X. Geng, F. Liu, J. Chen, S. Yang, T. P. Russell, L. Ding, *Sci.*

Bull. 62 (2017) 1494-1496.

[22] S. Dai, T. Li, W. Wang, Y. Xiao, T. Lau, Z. Li, K. Liu, X. Lu, X. Zhan, *Adv. Mater.* 30 (2018) 1706571.

[23] X. Shi, X. Liao, K. Gao, L. Zuo, J. Chen, J. Zhao, F. Liu, Y. Chen, A. K.-Y. Jen, *Adv. Funct. Mater.* 18 (2018) 1802324.

[24] Z. Yao, X. Liao, K. Gao, F. Lin, X. Xu, X. Shi, L. Zuo, F. Liu, Y. Chen, A. K. Y. Jen, *J. Am. Chem. Soc.* 140 (2018) 2054-2057.

[25] X. Liao, X. Shi, M. Zhang, K. Gao, L. Zuo, F. Liu, Y. Chen, A. K.-Y. Jen, *Chem. Commun.* 55 (2019) 8258-8261

[26] B. Fan, D. Zhang, M. Li, W. Zhong, Z. Zeng, L. Ying, F. Huang, Y. Cao, *Sci China Chem.* 62 (2019) 746-752.

[27] C. Yan, S. Barlow, Z. Wang, H. Yan, A. K.-Y. Jen, S. R. Marder, X. Zhan, *Nat. Rev. Mater.* 3 (2018) 18003.

[28] Q. Wang, Y. Qin, M. Li, L. Ye, Y. Geng, *Adv. Energy Mater.* 10 (2020) 2002572.

[29] J. Qu, Q. Zhao, J. Zhou, H. Lai, T. Liu, D. Li, W. Chen, Z. Xie, F. He, *Chem. Mater.* 31 (2019) 1664–1671.

[30] Z. Luo, R. Ma, Z. Chen, Y. Xiao, G. Zhang, T. Liu, R. Sun, Q. Zhan, Y. Zou, C. Zhong, Y. Chen, H. Sun, G. Chai, K. Chen, X. Guo, J. Min, X. Lu, C. Yang, H. Yan, *Adv. Energy Mater.* 10 (2020) 2002649.

[31] H. Chen, H. Lai, Z. Chen, Y. Zhu, H. Wang, L. Han, Y. Zhang, F. He, *Angew. Chem. Int. Ed.* 59 (2020) 2–11.

[32] H. Lai, H. Chen, J. Zhou, J. Qu, P. Chao, T. Liu, X. Chang, N. Zheng, Z. Xie, F. He, *iScience*

17 (2019) 302–314.

[33] H. Wang, T. Liu, J. Zhou, D. Mo, L. Han, H. Lai, H. Chen, N. Zheng, Y. Zhu, Z. Xie, F. He, *Adv. Sci.* 7 (2020) 1903784.

[34] Y. Lin, J. Wang, Z. G. Zhang, H. Bai, Y. F. Li, D. B. Zhu, X. W. Zhan, *Adv. Mater.* 27 (2015) 1170-1174.

[35] W. Zhao, S. Li, S. Zhang, X. Liu, J. Hou, *Adv. Mater.* 29 (2017) 1604059.

[36] K. Reichenbacher, H. I. Suss, J. Hulliger, *Chem. Soc. Rev.* 34 (2005) 22-30.

[37] N. Liang, W. Jiang, J. Hou, Z. Wang, *Mater. Chem. Front.* 1 (2017) 1291-1303.

[38] J. Zhang, H. Tan, X. Guo, A. Facchetti, H. Yan. *Nat. Energy* 3 (2018) 720-731.

[39] C. Li, H. Fu, T. Xia, Y. Sun, *Adv. Energy Mater.* 9 (2019) 1900999.

[40] X. Shi, L. Zuo, S. B. Jo, K. Gao, F. Lin, F. Liu, A. K. Y. Jen, *Chem. Mater.* 29 (2017) 8369-8376.

[41] X. Shi, J. Chen, K. Gao, L. Zuo, Z. Yao, F. Liu, J. Tang, A. K. Y. Jen, *Adv. Energy Mater.* 8 (2018) 1702831.

[42] T. Lu, F. Chen, *J. Comput. Chem.* 33 (2012) 580-592.

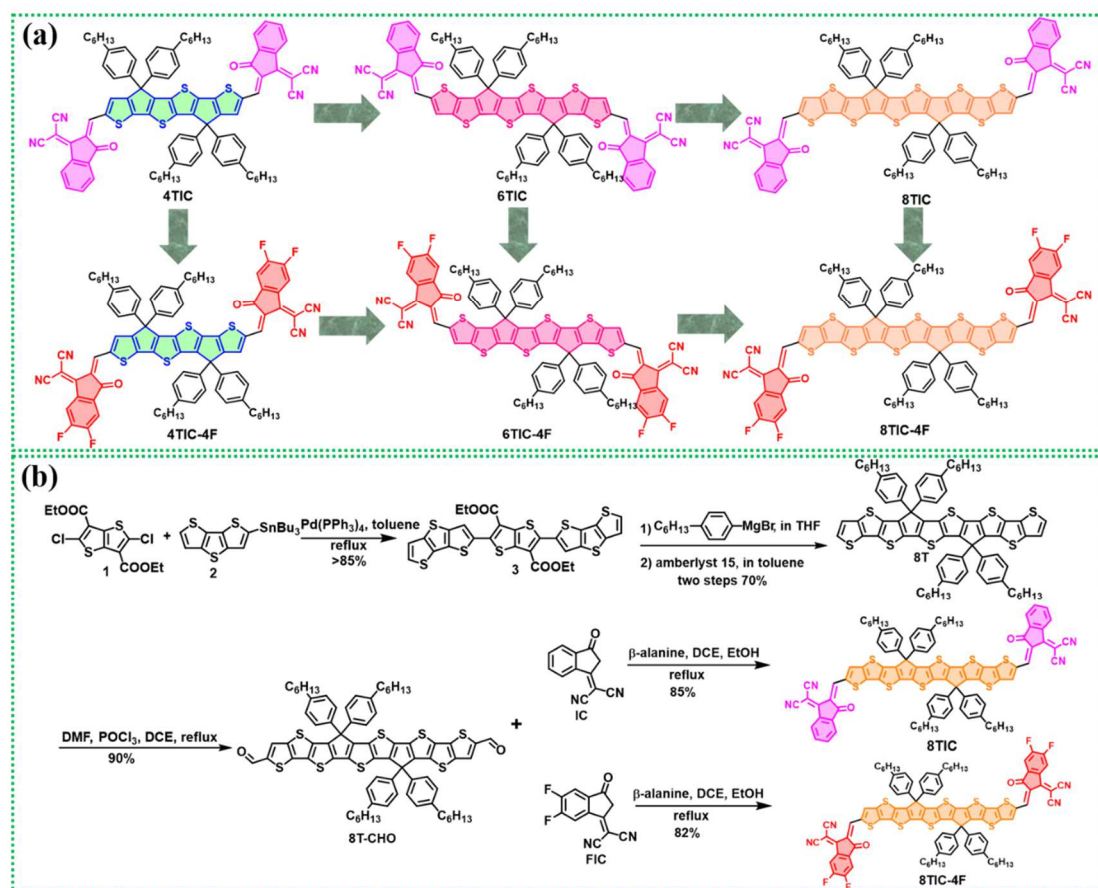
[43] Y. Cui, P. Zhu, X. Shi, X. Liao, Y. Chen, *J. Phys. Chem. C* 125 (2021) 10250-10259.

[44] C.-Z. Li, C.-C. Chueh, H.-L. Yip, K. M. O'Malley, W.-C. Chen, A. K.-Y. Jen, *J. Mater. Chem.* 22 (2012) 8574-8578.

[45] A. K. K. Kyaw, D. H. Wang, V. Gupta, W. L. Leong, L. Ke, G. C. Bazan, A. J. Heeger, *ACS Nano* 7 (2013) 4569-4577.

[46] R. Ingo, P. Jürgen, D. Vladimir, L. Laurence, V. Dirk, C. H. Jan, *Adv. Funct. Mater.* 14 (2014) 38.

- [47] J. Yuan, L. Qiu, Z. Zhang, Y. Li, Y. Chen, Y. Zou, *Nano Energy* 30 (2016) 312-320.
- [48] B. Collins, Z. Li, J. Tumbleston, E. Gann, C. McNeill, H. Ade, *Adv. Energy Mater.* 3 (2013) 65-74.
- [49] L. Ye, S. Zhang, W. Ma, B. Fan, X. Guo, Y. Huang, H. Ade, J. Hou, *Adv. Mater.* 24 (2012) 6335-6341.
- [50] C. Huang, X. Liao, K. Gao, L. Zuo, F. Lin, X. Shi, C.-Z. Li, F. Liu, Y. Chen, H. Chen and A. K.-Y. Jen, *Chem. Mater.* 30 (2018) 5429-5434.
- [51] W. Li, L. Ye, S. Li, H. Yao, H. Ade, J. Hou, *Adv. Mater.* 30 (2018) 1707170.



Scheme 1. (a) Molecular structures of non-fullerene acceptors 4TIC, 4TIC-4F, 6TIC, 6TIC-4F, 8TIC and 8TIC-4F. (b) The synthetic routes for 8TIC and 8TIC-4F.

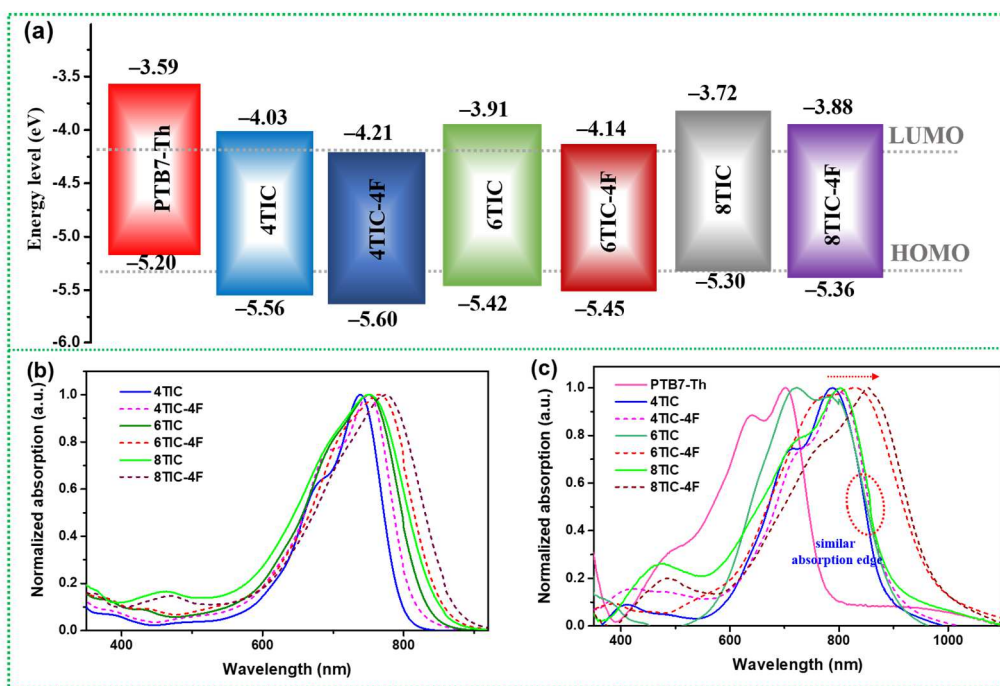


Figure 1. (a) Energy levels of donor and acceptors; Normalized UV-Vis-NIR spectra of acceptors in the dichloromethane solution (b) and thin film (c).

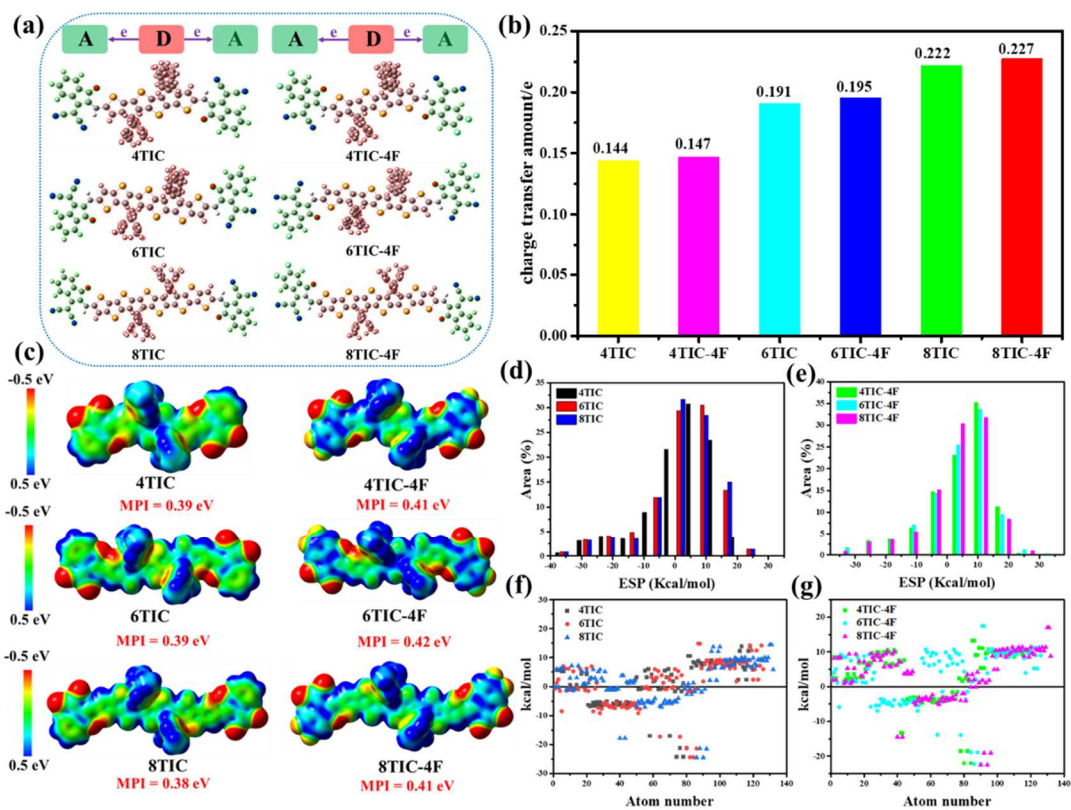


Figure 2. (a) Schematic diagram of charge transfer in various fragments, the red part is the electron-rich unit and the green part is the electron-deficient unit, (b) net charge transfer amount, (c) molecular ESP and MPI, (d)-(e) ESP area distributions and (f)-(g) average ESP value on each atom of the six acceptors.

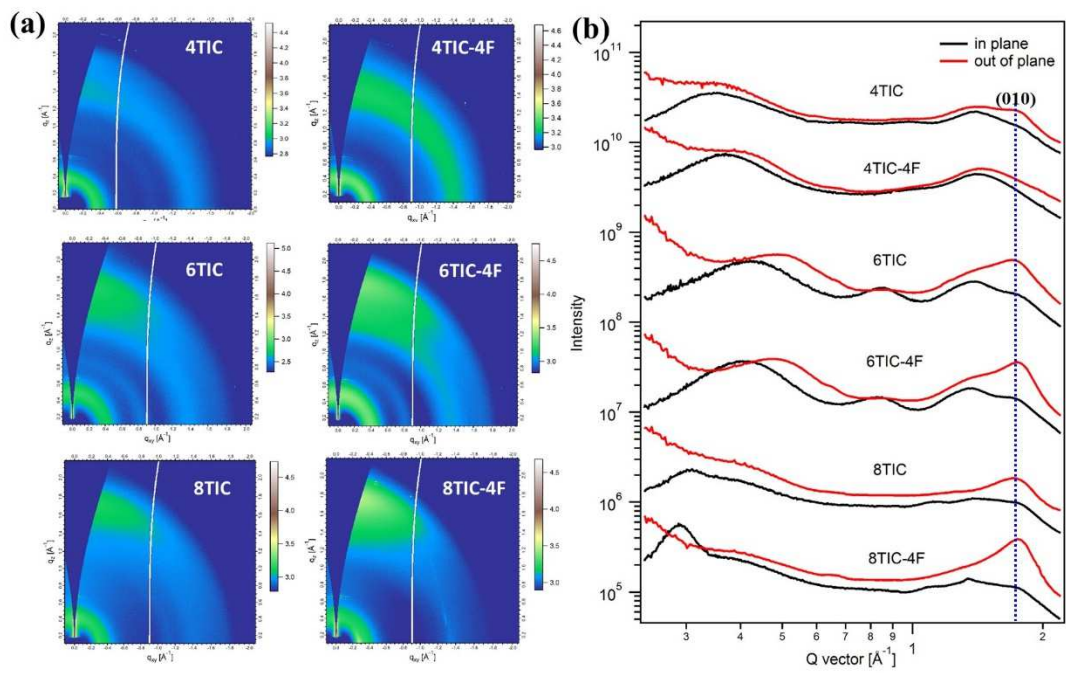


Figure 3. (a) 2D-GIWAXS patterns for acceptors neat film. (b) corresponding in-plane and out-of-plane cut line profiles.

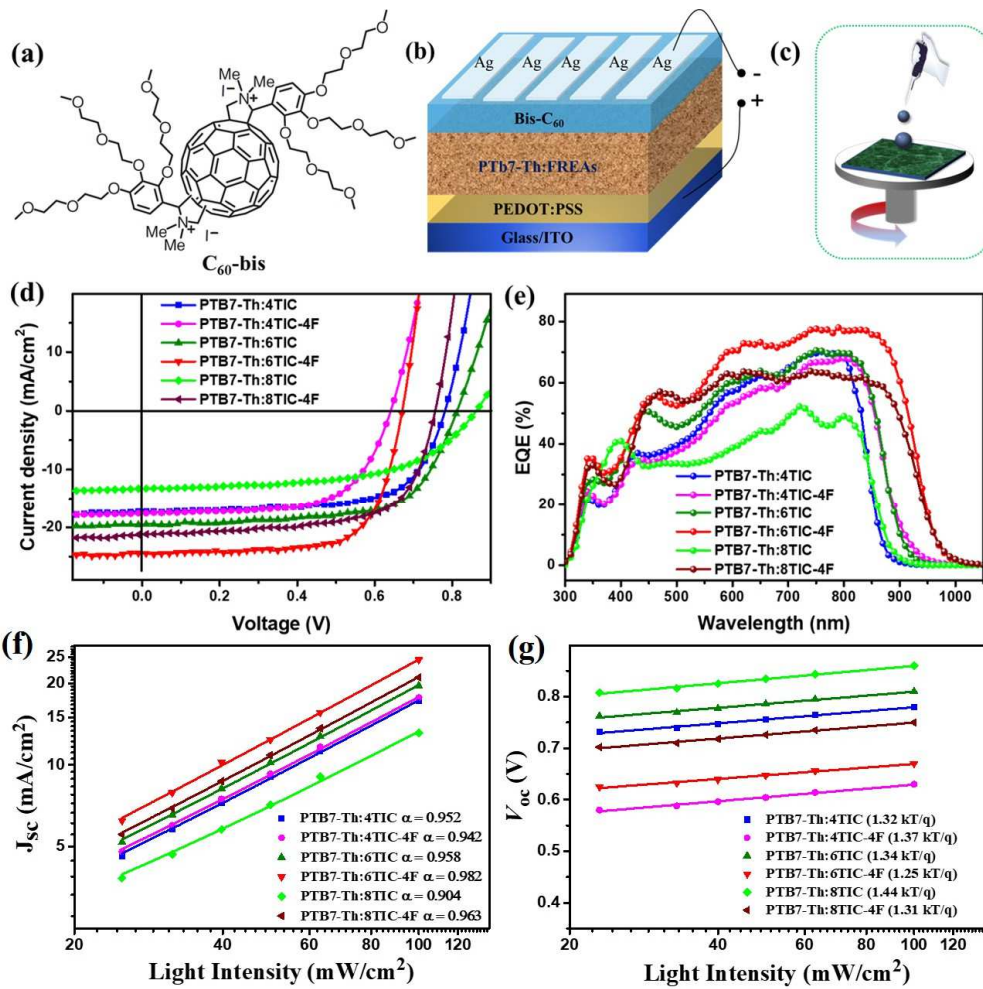


Figure 4. (a) Molecular structure of C_{60} -bis. (b) Device architecture. (c) Drop casting schematic diagram. (d) $J-V$ curves and (e) corresponding EQE spectra. Light intensity dependence of (f) J_{sc} and (g) V_{oc} .

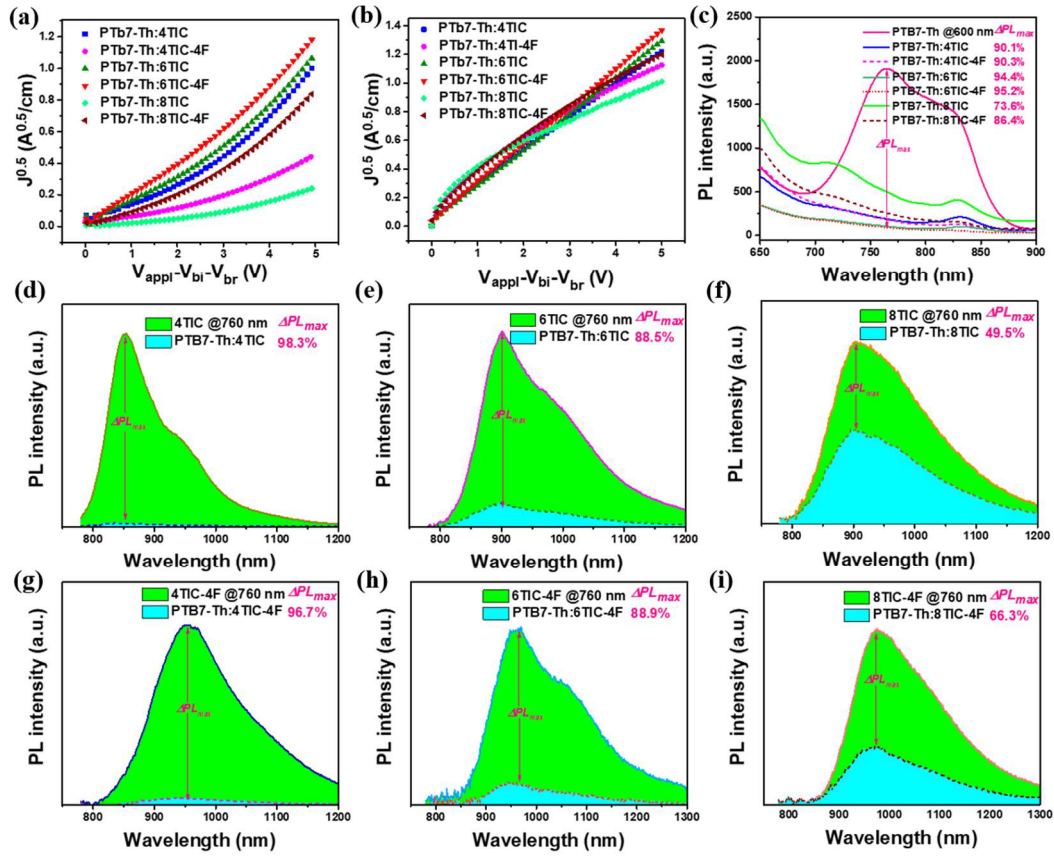


Figure 5. $J^{0.5}-V$ plots of (a) electron-only devices and (b) hole-only devices. (c) PL spectra of the pristine polymer film and active blend films with excitation wavelength at 600 nm. (d-i) PL spectra of the pristine acceptors film and active blend films with excitation wavelength at 760 nm.

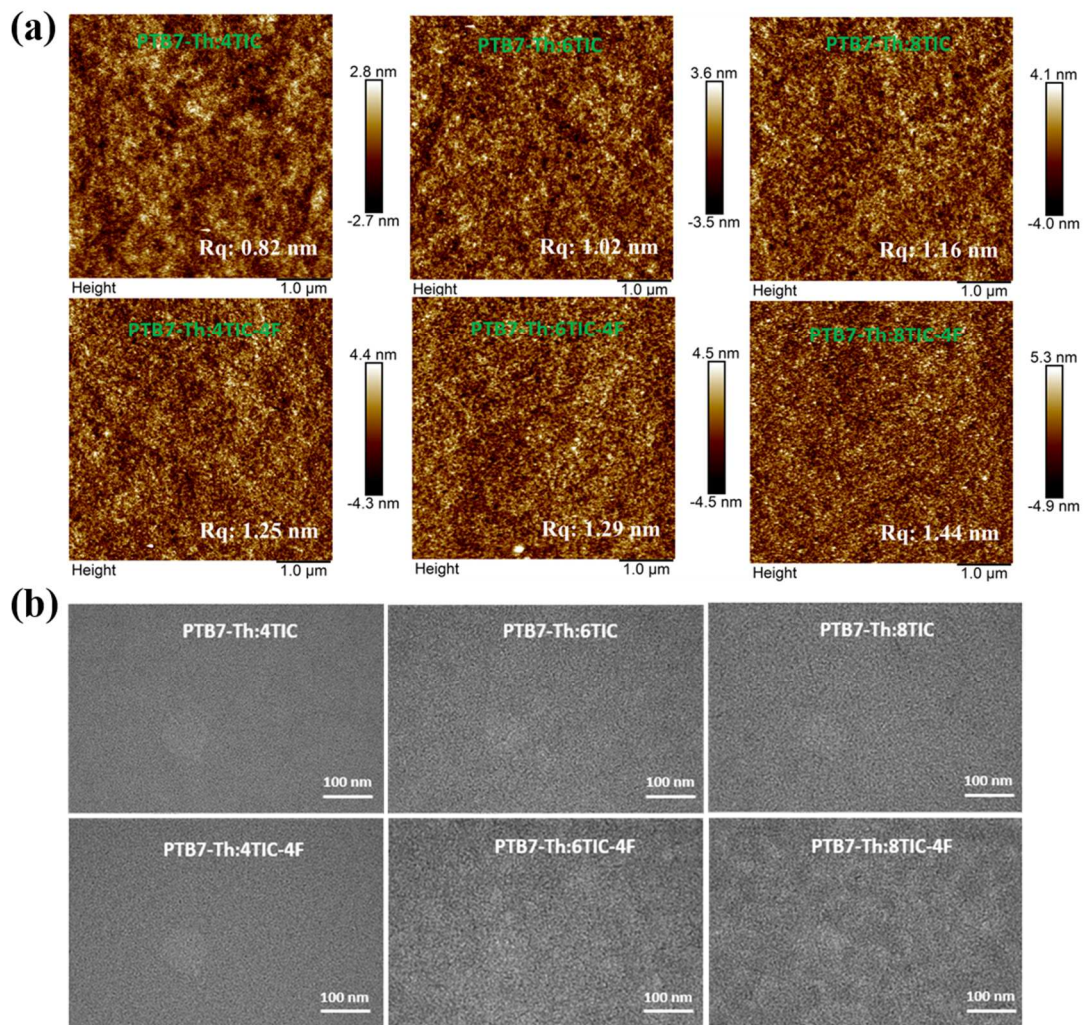


Figure 6. (a) AFM height images and (b) TEM images of the blend films.

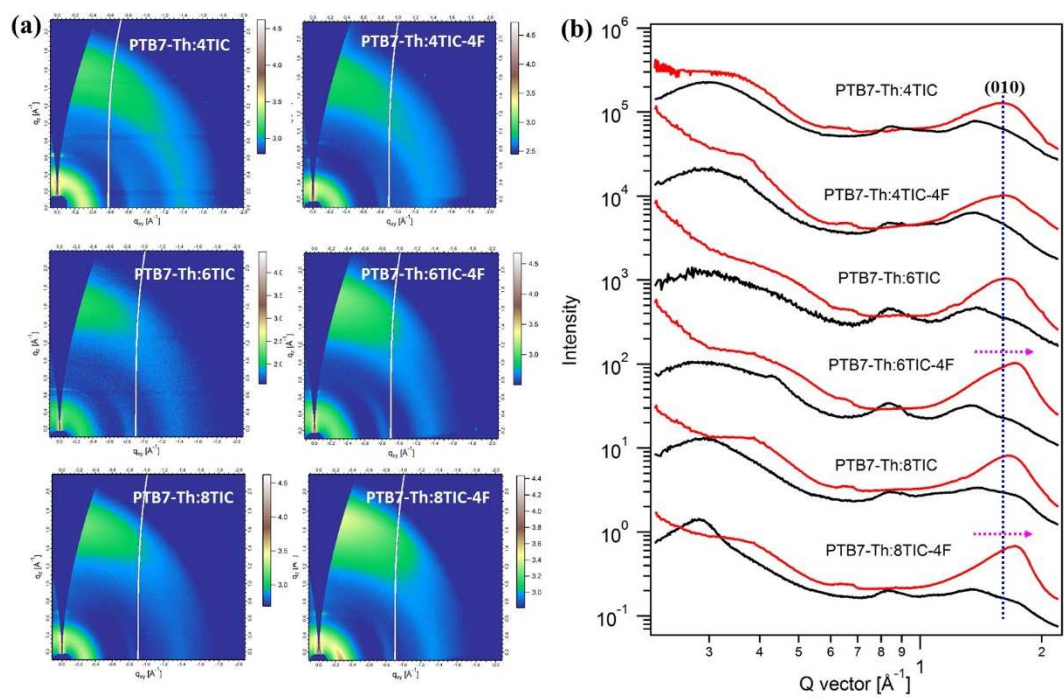


Figure 7. (a) 2D-GIWAXS patterns for blend film. (b) corresponding in-plane (black) and out-of-plane (red) cut line profiles.

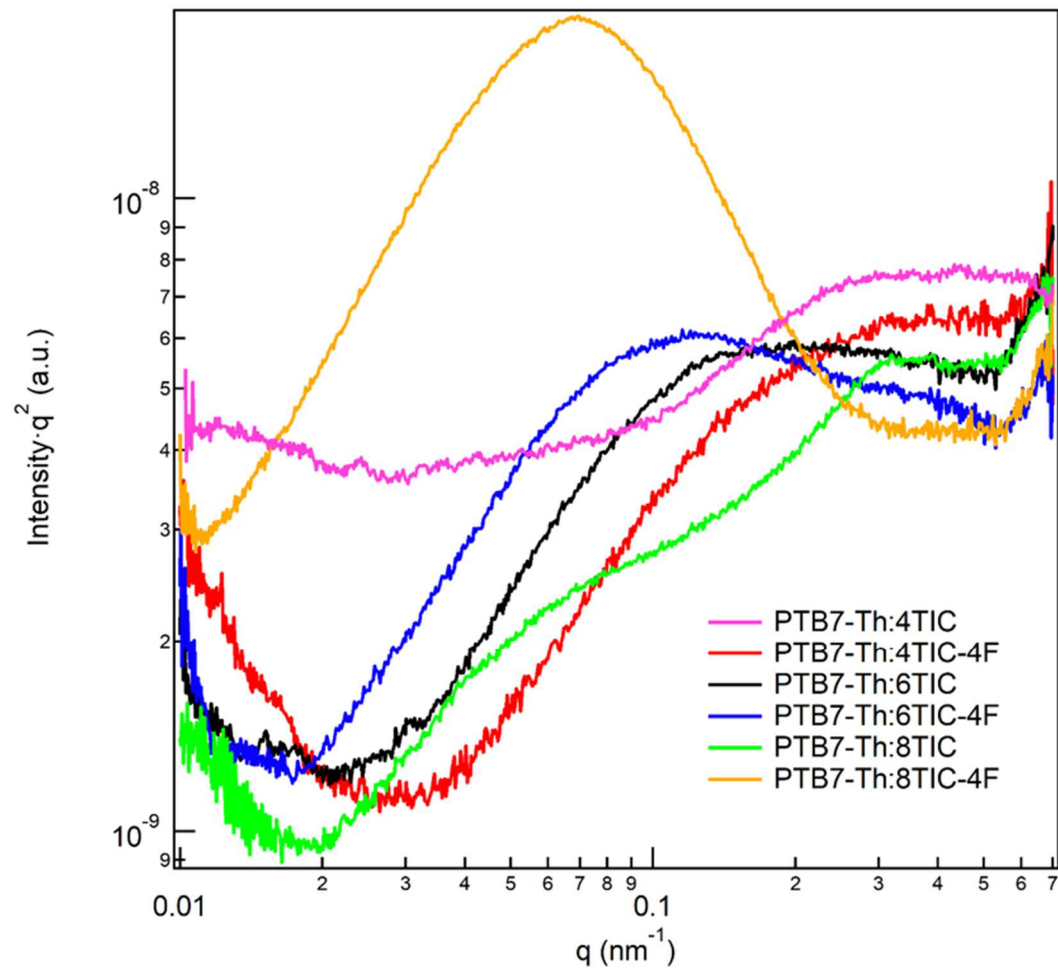


Figure 8. Resonant soft X-ray scattering of blend film.

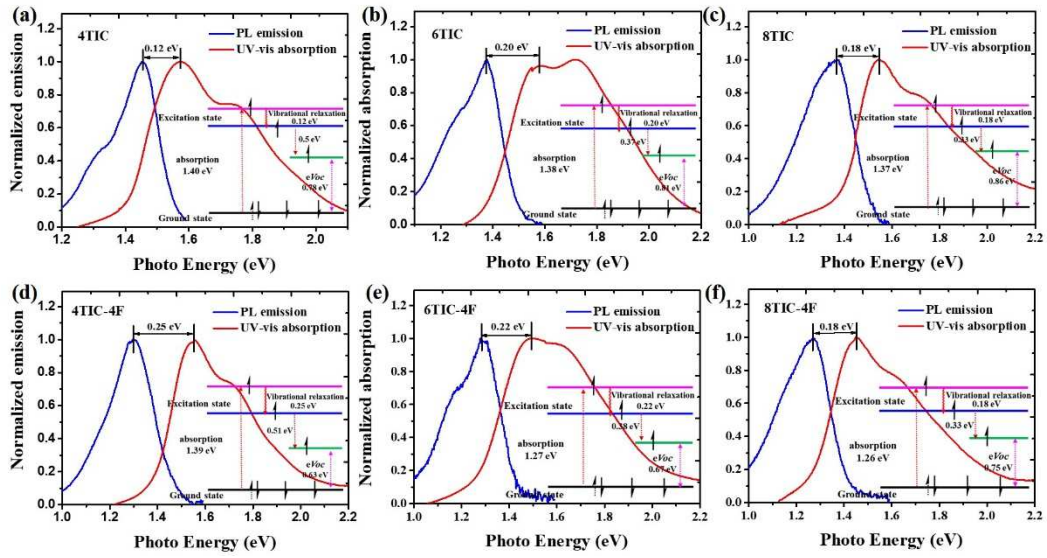


Figure 9. PL emission and UV-vis absorption spectra of (a) 4TIC, (b) 6TIC, (c) 8TIC, (d) 4TIC-4F, (e) 6TIC-4F, (f) 8TIC and (g) 8TIC-4F. Insets are the energy levels diagram of ground states and excitation states for the six systems devices.

Table 1. The basic properties of fused ring electron acceptors.

Acceptor	$\lambda_{\max}^a)$ (nm)	$\lambda_{\text{onset}}^a)$ (nm)	$\lambda_{\max}^b)$ (nm)	$\lambda_{\text{onset}}^b)$ (nm)	$E_g^c)$ (eV)	HOMO ^{d)} (eV)	LUMO ^{d)} (eV)	$E_g^e)$ (eV)	Ref.
4TIC	738	798 ± 2	788	886 ± 2	1.40	-5.56 ± 0.01	-4.03 ± 0.01	1.53	40
4TIC-4F	750	814 ± 2	799	890 ± 2	1.39	-5.60 ± 0.02	-4.21 ± 0.02	1.39	23
6TIC	750	826 ± 2	722	900 ± 2	1.38	-5.42 ± 0.02	-3.91 ± 0.02	1.51	41
6TIC-4F	765	856 ± 2	829	980 ± 2	1.27	-5.45 ± 0.01	-4.14 ± 0.01	1.31	23
8TIC	752	850 ± 2	802	902 ± 2	1.37	-5.30 ± 0.02	-3.72 ± 0.02	1.58	This work
8TIC-4F	774	872 ± 2	854	984 ± 2	1.26	-5.36 ± 0.01	-3.88 ± 0.01	1.48	This work

^{a)}In dichloromethane solution; ^{b)}In neat film; ^{c)}Calculated from empirical formula: $E_g = 1240/\lambda_{\text{onset}}^b)$; ^{d)}measured by cyclic voltammetry (CV) method; ^{e)}Calculated from equation: $E_g = E_{\text{HOMO}}^d) - E_{\text{LUMO}}^d)$

Table 2. Photovoltaic parameters of OSCs based on PTB7-Th:FREAs. Average values obtained from 10 devices are shown in parentheses.

Active layer	V_{oc} (V)	J_{sc} (mA/cm ²)	FF	PCE (%)	μ_h ($\times 10^{-4}$ cm ² V ⁻¹ s ⁻¹) ^a	μ_e ($\times 10^{-4}$ cm ² V ⁻¹ s ⁻¹) ^a	μ_h/μ_e	E_{loss} (eV) ^b
PTB7-Th:4TIC	0.78 (0.78±0.01)	17.3 (17.2±0.3)	0.66 (0.65±0.02)	8.91 (8.66±0.21)	2.46 (2.41±0.12)	1.62 (1.57±0.09)	1.52	0.62 (0.62±0.01)
PTB7-Th:4TIC-4F	0.63 (0.62±0.01)	17.7 (17.6±0.4)	0.65 (0.64±0.02)	7.25 (7.05±0.16)	1.80 (1.8±0.08)	3.17 (3.12±0.12)	5.68	0.76 (0.76±0.01)
PTB7-Th:6TIC	0.81 (0.80±0.01)	19.6 (19.7±0.3)	0.65 (0.64±0.02)	10.32 (10.03±0.21)	2.81 (2.75±0.06)	1.91 (1.86±0.08)	1.47	0.57 (0.57±0.01)
PTB7-Th:6TIC-4F	0.67 (0.66±0.01)	24.4 (24.3±0.4)	0.71 (0.69±0.02)	11.61 (11.22±0.28)	3.15 (3.11±0.12)	2.42 (2.38±0.06)	1.30	0.60 (0.60±0.01)
PTB7-Th:8TIC	0.86 (0.85±0.01)	13.1 (13.0±0.2)	0.55 (0.54±0.02)	6.20 (5.88±0.15)	1.23 (1.19±0.06)	0.105 (0.103±0.005)	11.71	0.51 (0.51±0.01)
PTB7-Th:8TIC-4F	0.75 (0.74±0.01)	21.0 (20.9±0.4)	0.66 (0.65±0.02)	10.40 (10.02±0.23)	2.21 (2.12±0.11)	1.26 (1.22±0.08)	1.75	0.51 (0.51±0.01)

^aMeasured by space charge limited current (SCLC) method; ^bEnergy losses derived

from formula $E_{loss} = E_g^{opt} - eV_{oc}$.

Table 3. Morphological parameters obtained from GIWAXS and RSoXS.

Samples	(100) in-plane			(010) out-of-plane			RSoXS		
	Location	d-spacing ^{a1}	CL ^{b1}	Location	d-spacing ^{a1}	CL ^{b1}	q	Domain spacing ^{c1}	Domain size
	(Å ⁻¹)	(Å)	(Å)	(Å ⁻¹)	(Å)	(Å)	(nm ⁻¹)	(nm)	(nm)
PTB7-Th:4TIC	0.301 ±	20.86	39.9	1.368 ±	4.59	11.4	0.277 ±	22.67	11.34
	0.0002			0.0036			0.0032		
PTB7-Th:4TIC-4F	0.296 ±	21.22	46.9	1.423 ±	4.41	22.0	0.390 ±	16.10	8.05
	0.0006			0.0060			0.0325		
PTB7-Th:6TIC	0.293 ±	21.43	40.1	1.405 ±	4.47	9.8	0.178 ±	35.28	17.64
	0.0015			0.0301			0.0025		
PTB7-Th:6TIC-4F	0.294 ±	21.36	47.8	1.582 ±	3.97	15.1	0.124 ±	50.65	25.33
	0.0010			0.0028			0.0003		
PTB7-Th:8TIC	0.290 ±	21.66	58.8	1.384 ±	4.54	10.1	0.236 ±	26.6	13.3
	0.0004			0.0114			0.0579		
PTB7-Th:8TIC-4F	0.279 ±	22.51	88.6	1.562 ±	4.02	18.2	0.067 ±	93.73	46.87
	0.0003			0.0032			0.0001		

^{a1}Calculated from $d = 2\pi/q$, where q is the location of the (100) or (010) diffraction peak; ^{b1}Obtained from Scherrer equation: $CL = 2\pi K/\Delta q$, where Δq is the full-width at the half-maximum of the peak and K is the Scherrer factor; ^{c1}Calculated from $d = 2\pi/q$, where q is the location of maximum peak of RSoXS profile.

A new fused core with eight thiophene rings (8T) was designed and synthesized, which was end-capped with IC or fluorinated IC (DFIC) to afford two new FREAs, 8TIC and 8TIC-4F. These two new FREAs, together with previously reported 4T and 6T based FREAs 4TIC, 4TIC-4F, 6TIC and 6TIC-4F to construct a library of structurally closely related FREAs. With this small library, this work systematically investigated the synergistic effect of central core-extension, fluorination, and their combined effects on A-D-A type NIR NFAs.

Keyword: ultra-narrow bandgap, nonfullerene acceptors, intramolecular charge transfer, core and end group, organic solar cells

X. Liao, H. Pei, H. Zhao, Y. Cui, L. Li, X. Shi, P. Zhu*, Wei Ma*, Yiwang Chen*, A. K.-Y. Jen*

The Synergistic Effects of Central Core Size and End Group Engineering on Performance of Narrow Bandgap Nonfullerene Acceptors

ToC figure

